

1 **INNOVATIVE STABILIZATION TECHNIQUES FOR WEAK CRUSHED ROCKS**
2 **USED IN ROAD UNBOUND LAYERS: A LABORATORY INVESTIGATION**

3
4
5 **Diego Maria Barbieri, Corresponding Author**

6 Norwegian University of Science and Technology,
7 Department of Civil and Environmental Engineering.
8 Høgskoleringen 7A, Trondheim, 7491, Trøndelag, Norway
9 Tel: +47 930 02 908; Email: diego.barbieri@ntnu.no

10
11 **Inge Hoff**

12 Norwegian University of Science and Technology,
13 Department of Civil and Environmental Engineering.
14 Høgskoleringen 7A, Trondheim, 7491, Trøndelag, Norway
15 Email: inge.hoff@ntnu.no

16
17 **Mai Britt Engeness Mørk**

18 Norwegian University of Science and Technology,
19 Department of Geosciences and Petroleum.
20 Sem Sæalandsvei 1, Trondheim, 7491, Trøndelag, Norway
21 Email: mai.britt.mork@ntnu.no

22
23
24 Declarations of interest:

25 none

26
27 Re-submission date:

28 20/11/2018
29
30
31
32
33
34
35
36
37
38
39
40
41
42
43
44
45
46
47

48 **ABSTRACT**

49 The “Ferry-free coastal highway route E39” project includes building several long tunnels
50 along the southwestern Norwegian coast. The tunnelling operations will generate a large
51 quantity of blasted rocks; these could be used in the road unbound layers close to the place of
52 production to provide a sustainable cost-benefit application. The existing design guidelines
53 define strength requirements for road unbound layers in terms of Los Angeles and micro-Deval
54 tests. Even if the major part of the rocks has igneous origin and could potentially fulfil the
55 standard tests, the damage induced by the confined heavy blasting makes the materials fail the
56 check procedures. The research investigates how to enable the use of the “weak” rocks by
57 investigating three possible techniques. The first approach is the mixture between the different
58 types of rocks available in situ. The second approach is additive application; two different non-
59 traditional additive types are examined: one is polymer-based, the other one is lignin-based.
60 The third approach is the attempt to modify the rocks mineralogical structure by overheating.
61 The research test campaign uses both the aforementioned standard tests and repeated triaxial
62 load tests. Rocks mixture and additives application are viable and sustainable methods to
63 improve the mechanical properties of the “weak” crushed metamorphic rocks. Overheating
64 does not turn out to be an effective and convenient procedure.

65

66 Keywords: Stabilization, Crushed rock, Pavement unbound, Los Angeles test, Micro-Deval
67 test, Repeated triaxial load test.

68

69

70

71

72

73

74

75

76

77

78

79

80

81

82

83

84

85

86

87

88

89

90

91

92

93

1 INTRODUCTION AND BACKGROUND

Norwegian Public Roads Administration (NPRA) is currently running the “Ferry-free coastal highway route E39” project, which improves the viability along the southwestern Norwegian coast for a total length of about 1100 km from Trondheim to Kristiansand (NPRA, 2017). The project includes the building of several bridges and tunnels, while aiming for creating a sustainable infrastructure. The project is crucial to regional and national development as the industries located along the route generate about half of Norway’s traditional export (Dunham, 2016).

The extended tunnelling systems will generate a very large quantity of blasted rocks. They could potentially be used as viable substitutes for natural aggregates in the road unbound layers close to the place of production. Previous experience regarding the recycling strategies of tunnel excavation materials highlighted the importance of this challenge for construction management and economics (Burdin and Monin, 2009; Haritonovs et al., 2016; Lieb, 2009; Resch et al., 2009).

Using the excavated geomaterials is beneficial from economic, environmental and social points of views (Chittoori et al., 2012; Petkovic, 2005; Riviera et al., 2014); energy consumption reduction and limited greenhouse gas emissions are the most beneficial advantages (Aatheesan et al., 2008; Arulrajah et al., 2013; Gomes Correia et al., 2016; Núñez et al., 2008). The usage of blasted materials in pavement applications is a sustainable solution to minimise the waste while reducing the demand for scarce quarried materials, activity which is resource intensive and consumes large amounts of energy (Fladvad et al., 2017). The transport distance of the blasted and crushed rocks should be within 20 - 30 km to represent a competitive solution compared to the purchase of quarry virgin aggregates (Berger, 1978; Neeb, 1992). Furthermore, the concern about environmentally-friendly and sustainable constructions is becoming more and more relevant in Norway, as it pledges to become climate neutral by 2030 (Teknologirådet, 2012).

The existing strength requirements for road unbound layers are connected to relatively simple tests: the Norwegian pavement design manual N200 (NPRA, 2014a) sets limits in terms of grain shape (CEN, 2012a), flakiness index value (CEN, 2012b), Los Angeles (LA) value (CEN, 2010) and micro-Deval (MDE) value (CEN, 2011). By respecting the specified thresholds, the road is expected to perform adequately without encountering premature damage (Barbieri et al., 2017).

The goal of the research is to explore techniques to improve the mechanical properties of the crushed rocks not complying with the standard requirements; the aim is to enable their use in the road unbound layers close to the place of production. This would entail savings on the consumption of natural resources and transport reduction; thus promoting a beneficial impact on sustainability.

The research examines mechanical and chemical treatments to make the weak materials suitable for the application. Three types of crushed rocks are chosen and investigated. One type meets the code requirements (“strong” rocks), while the other two do not (“weak” rocks); XRD diffractometer (XRD) analyses describe the mineralogy.

The first studied technique is to mix the weak rocks with the strong ones available in situ. The second considered approach is additive application. Currently there are several stabilization methods, i.e. cement, bitumen, lime, fly ash, gypsum (Arulrajah et al., 2016; Behnood, 2018; Jiang and Fan, 2013; Mohammadinia et al., 2017; Myre, 2014; NPRA, 2014b; Siripun et al., 2010). Two non-traditional stabilization techniques are examined: one is

141 polymer-based and the other one is lignin-based. The third investigated method is to overheat
 142 the rocks to check for any possible induced changes in the mineralogical composition, which
 143 may strengthen the rocks. Both the standard tests (LA and MDE) and Repeated Triaxial Load
 144 Tests (RTLTs) are used to assess the materials performance.

145

146 **2 METHODOLOGY**

147

148 **2.1 MATERIALS INVESTIGATED**

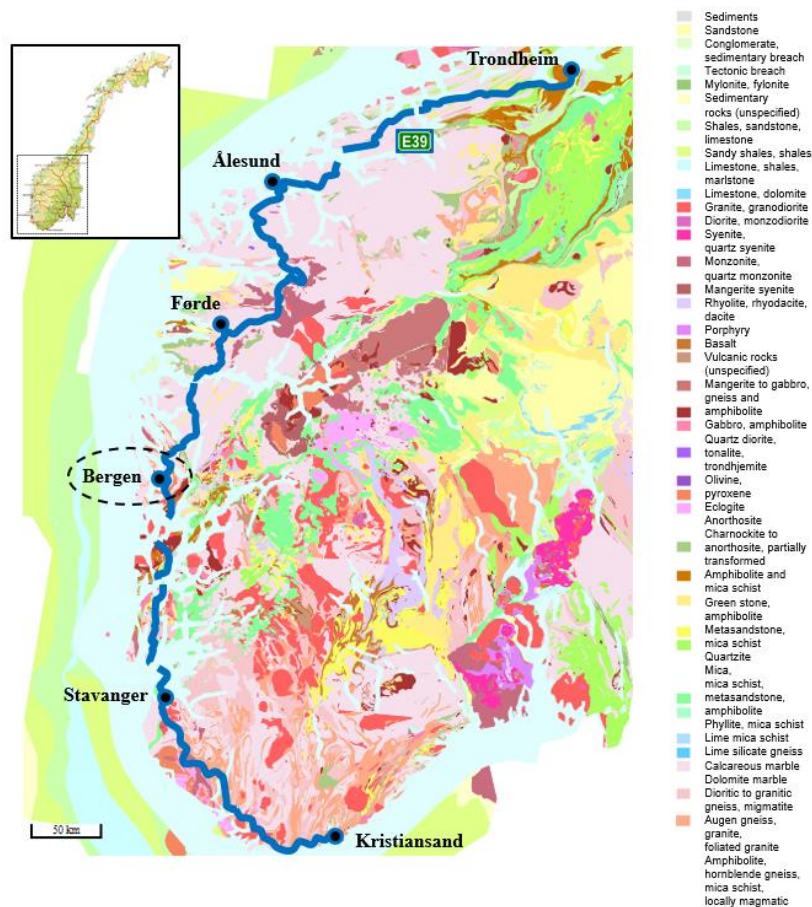
149

150 **2.1.1 GEOLOGICAL CHARACTERIZATION**

151

152 The E39 highway alignment comes across different types of bedrocks (NGU, 2017; Ramberg
 153 et al., 2013). The major part of the rocks is igneous and supracrustal of Precambrian ages (1700
 154 - 900·10⁶ years) variably influenced by metamorphism and deformation related to the
 155 Caledonian orogeny. They mainly comprise granite, granodiorite and granitic to dioritic gneiss.
 156 There are also areas with Caledonian rocks; these locations are anyway at maximum 20 - 30
 157 km far from the most widespread aforementioned geology. Metamorphic rocks occur close to
 158 Bergen (gabbro and augen gneiss). Zones of foliated Caledonian metamorphic rocks (e.g. mica-
 159 schist and phyllite) are locally present, in particular around Boknafjord area close to Stavanger.
 160 Three types of crushed rocks produced by the current tunnel excavations close to Bergen are
 161 investigated: they properly represent the variety in the geology spread along the entire highway
 162 alignment (Barbieri et al., 2019) as shown in Figure 1.

163



164

165

Fig. 1. E39 highway alignment and bedrock geology (Barbieri et al., 2019).

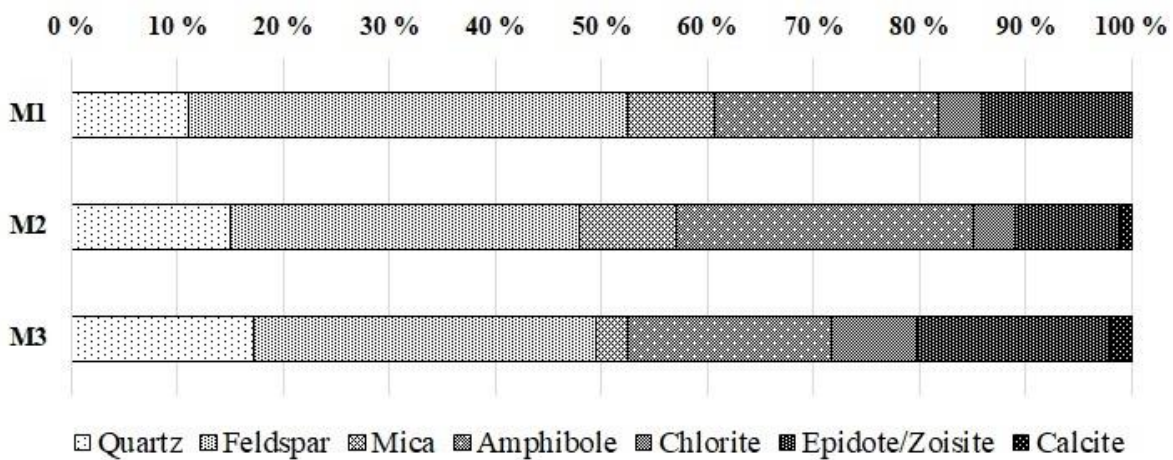
166 The three materials are denominated M1, M2 and M3, all being mixtures of different local
167 rocks:

168
169 - Material M1. Mafic igneous origin, partly modified by metamorphism (amphibolite), minor
170 amounts of felsic gneisses and mica-schist.

171 - Material M2. Metamorphic origin, fine-grained felsic and micaceous rocks.

172 - Material M3. Metamorphic origin, very fine-grained felsic and micaceous rocks.
173

174 Batches of each material type are prepared for XRD diffractometer analyses to identify the
175 main mineralogical compositions according to Rietveld mineral quantification. Samples are
176 crushed, split, milled to 10µm and analysed as powder prepare in the XRD diffractometer.
177 Figure 2 displays semi-quantitative weight proportions of the most abundant minerals.
178



179
180
181

Fig. 2. Bulk mineralogy of the investigated crushed rocks.

182 Quartz, feldspar and amphibole are the predominant minerals in all M1, M2 and M3 mixtures
183 (and main constituents of amphibolites and gneisses). M3 is richer in chlorite, epidote-zoisite
184 and calcite compared to M1 and M2. Moreover, M3 has a higher content of foliated felsic rocks:
185 networks of fine epidote-zoisite particles partly replace feldspars. Igneous rocks M1 are
186 modified by metamorphism, e.g. amphibolization and replacement of coarse igneous feldspar
187 by aggregates of fine epidote and feldspar. Finer-grained felsic and micaceous rocks appear
188 more dominant in M2 and especially in M3.
189

190 2.1.2 STANDARD TESTS CHARACTERIZATION

191

192 The pavement design manual N200 (NPRA, 2014a) sets requirements for the use of crushed
193 rocks. It is possible to use this resource in the road base layer as paved crushed rocks and in
194 the road subbase layer as unsorted crushed rocks if Los-Angeles (LA) standard test (CEN, 2010)
195 and micro-Deval (MDE) standard test (CEN, 2011) are fulfilled. The LA limit values are
196 respectively 30 and 35 for base layer and subbase layer, the MDE limit value is 15 for both of
197 them. Further requirements in terms of upper and lower grain size distribution curve are
198 demanded for the base layer (Figure 3). The grain size distribution curve of the subbase layer
199 must be within 20/120 mm.

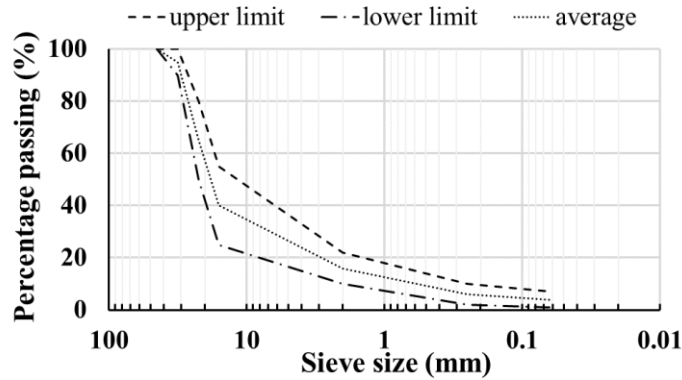


Fig. 3. Grain size distribution limit curves for base layer.

200
201
202
203
204
205
206

Figure 4 displays the materials values related to LA and MDE standard check procedures. Material M1 fulfils the code requirements. Both materials M2 and M3 have LA values lying close to the limit, and exceed the threshold regarding MDE values. Material M1 is designated as “strong” and materials M2 and M3 are designated as “weak” in the research.

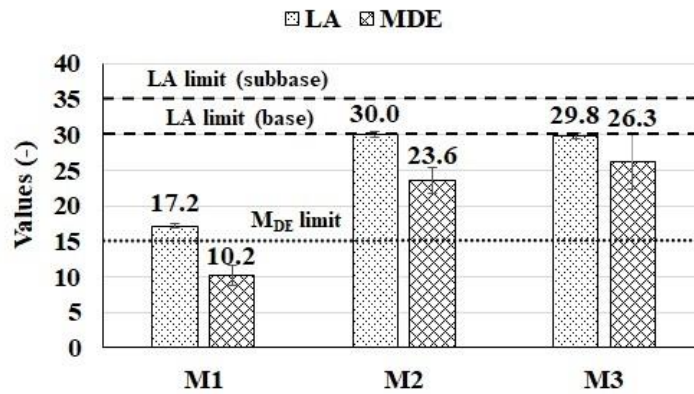


Fig. 4. Los Angeles and micro-Deval values of investigated materials (Barbieri et al., 2019).

207
208
209
210
211

2.1.3 REPEATED TRIAXIAL LOAD TEST

The Repeated Triaxial Load Test (RTL) gives a comprehensive insight into material properties by assessing the stiffness and the resistance to permanent deformation (CEN, 2004). RTL is one of the best methods available for laboratory simulation of traffic loading on unbound granular materials (UGMs); it reproduces the stress conditions in flexible pavements more adequately than other available methods like the CBR test (Barksdale, 1971). UGMs behaviour is connected to the following parameters: stress level, moisture content, dry density, grading and mineralogy, etc. (Lekarp et al., 2000a, 2000b; Uthus et al., 2007).

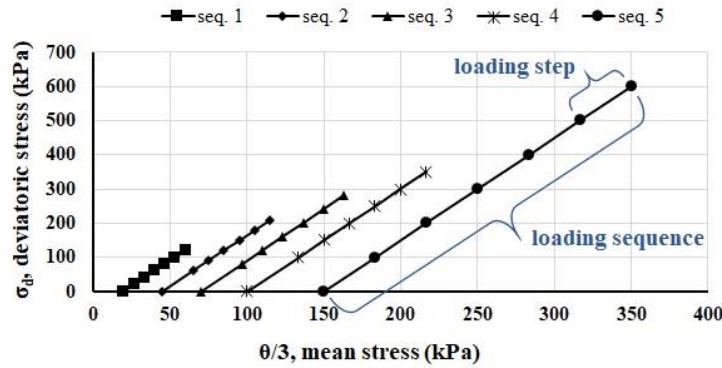
The preparation of the specimen follows a defined procedure. Firstly, 7300 g of material is prepared according to the grading curve displayed in Figure 3. The amount of fines content, namely the material passing the 0.0063 mm sieve, is equal to 292 g. Consequently, the desired amount of water, and additive if needed by the test, is added. The mixture is divided into four parts and rests in as many impermeable bags for 24 h. The operator then compacts the four layers inside a steel mould; the bulk density and dry density are assessed (CEN, 2003).

The optimum moisture content (OMC) evaluated for all the materials M1, M2 and M3 is $w=5\%$. A Kango 950X vibratory hammer (total weight 35 kg, frequency 25 - 60 Hz, amplitude 5 mm) is used to compact the layers inside the mould, the compaction time is 30 s

225
226
227

228 per layer. All the samples have a diameter of 150 mm and the final height varies between 170
 229 and 190 mm. The sample height differs from the indication given by the code, where the height
 230 is recommended to be twice the diameter of the sample (CEN, 2004). Research regarding the
 231 influence of the height to diameter ratio with respect both to resilient modulus and permanent
 232 deformations demonstrates that samples with a ratio ranging from 1:1 to 1.5:1 show little
 233 differences (Dongmo-Engeland, 2005).

234 RTLT apparatus exerts a uniform confining pressure in all the directions (σ_t , triaxial or
 235 confining stress) and an additional vertical dynamic stress (σ_d , deviatoric stress), which
 236 stepwise increases at different levels of σ_t . The RTLT apparatus performs the multi-stage low
 237 stress level (MS LSL) loading procedure: five sequences are associated with five different σ_t
 238 values ($\sigma_t = 20, 45, 70, 100, 150$ kPa). In addition, six steps associated to six given σ_d values
 239 form each sequence (CEN, 2004). Figure 5 displays the five loading sequences and the
 240 respective loading increments according to bulk stress θ ($\theta = \sigma_1 + \sigma_2 + \sigma_3 = \sigma_d + 3\sigma_t$; $\sigma_1, \sigma_2,$
 241 σ_3 are principal stresses) and σ_d . Each load step consists of 10,000 load pulses at 10 Hz
 242 frequency. A loading sequence is interrupted if the axial permanent deformation reaches 0.5%.
 243 Pressurised water is the confining medium; a hydraulic jack exerts σ_d according to a sinusoidal
 244 pattern, a minimum value of 5 kPa assures contact between the specimen end plate and the jack.
 245



246
 247
 248
 249

Fig. 5. Loading sequences for the MS LSL procedure.

250 The resilient modulus M_R associated with a change in the dynamic deviatoric stress σ_d^{dyn} and
 251 constant σ_t is defined as follows

252

$$253 \quad M_R = \frac{\Delta\sigma_d^{dyn}}{\varepsilon_a^{el}}, \quad (1)$$

254

255 where ε_a^{el} is the axial resilient strain. Several non-linear relationships have been proposed to
 256 describe M_R with reference to bulk stress θ (Lekarp et al., 2000a). The following k- θ
 257 relationship is adopted (Hicks and Monismith, 1971)

258

$$259 \quad M_R = k_1 \sigma_a \left(\frac{\theta}{\sigma_a} \right)^{k_2}, \quad (2)$$

260

261 where σ_a is a reference pressure (100 kPa) and k_1, k_2 are regression parameters. The relationship
 262 enables a clear comparison in two-dimensional plots between the materials performances.

263 The permanent deformation is investigated through the Coulomb approach (Hoff et al.,
 264 2003). The Coulomb criterion relates the mobilized shear strength to the development of
 265 permanent deformations and the maximum shear strength to incremental failure. The mobilized
 266 angle of friction ρ and the angle of friction at incremental failure φ respectively express the
 267 degree of mobilized shear strength and the maximum shear strength. The angle of friction and
 268 the angle of friction at incremental failure identify three different ranges of material behaviour:
 269 elastic, elasto-plastic and failure. The strain rate $\dot{\epsilon}$ is a measure of the speed of the permanent
 270 deformation; this parameter refers to the development of permanent deformation per cycle.
 271 Table 1 defines the two boundary lines between the three aforementioned ranges: each load
 272 step is categorised considering the average strain rate for the cycles from 5000 to 10,000 (Hoff
 273 at al. 2003).
 274

Permanent strain rate	Range
$\dot{\epsilon} < 2.5 \cdot 10^{-8}$	elastic zone
$2.5 \cdot 10^{-8} < \dot{\epsilon} < 1.0 \cdot 10^{-7}$	elasto-plastic zone
$\dot{\epsilon} > 1.0 \cdot 10^{-7}$	plastic (incremental failure) zone

275
 276 Table 1. Permanent strain rate values defining the material range boundary lines.
 277

278 The equations defining the elastic limit line and incremental failure line are respectively
 279

$$280 \sigma_d = \frac{2 \sin \rho (\sigma_3 + a)}{1 - \sin \rho}, \quad (3)$$

$$281 \sigma_d = \frac{2 \sin \varphi (\sigma_3 + a)}{1 - \sin \varphi}; \quad (4)$$

282
 283 a regression analysis is used to assess the boundary lines. As a simplification, the apparent
 284 attraction a is assumed to be 20 kPa for all the samples (Uthus et al., 2007).
 285
 286

287 2.2 TECHNIQUES TO IMPROVE THE MECHANICAL PROPERTIES

288
 289 The research investigates different approaches to improve the mechanical properties of the
 290 “weak” metamorphic rocks, namely materials M2 and M3. Both standard tests and RTLTS
 291 evaluate the performance related to the assessed techniques. Replicate specimens are used and
 292 average results are estimated: two samples for a MDE test (each MDE test requires a double
 293 sample in turn), three samples for a LA test and two samples for a RTLTS are considered for
 294 each testing condition described below.
 295

296 2.2.1 MIXTURE OF THE ROCKS AVAILABLE IN SITU

297
 298 The major part of the rocks spread along the highway alignment have mafic igneous origin and
 299 are suitable for road construction; therefore, a convenient solution could be to mix
 300 appropriately the different rock types that are available in situ. Material M1 is mixed with
 301 materials M2 or M3 according to three proportions in mass (25%, 50%, 75%). LA and MDE
 302 tests respectively express resistance against fragmentation and wearing (Erichsen et al., 2011):
 303 these standard procedures validate the appropriateness of the mixing approach.

304 **2.2.2 POLYMER-BASED ADDITIVE APPLICATION**

305

306 The tested polymer-based additive is water-soluble, non-leachable and UV, heat stable. The
307 additive is a nanoscale technology and is made of two components C1 and C2; the additive
308 modifies the rocks' surfaces and mechanical improvements can be measured at a macroscale
309 level (Huang and Wang, 2016; Paul and Robeson, 2008; Roco, 2003; Sobolev and Shah, 2015).

310 Component C1 is an acrylic co-polymer emulsion based on acetic acid and methanol.
311 The particle size is lower than 90 nm and has almost the same number of polymer particles as
312 soil particles. Component C2 is a polymeric dispersion based on propylene glycol and alkoxy-
313 alkyl silyl. After hydrolysis, the formed silanol (Si-OH) group can condense with another
314 silanol group belonging to the silicate-containing surface of the rocks and form a siloxane
315 linkage (= Si-O-Si=), namely a strong chemical covalent polar bond. Therefore, component C2
316 converts the water absorbing silanol groups presented on the rocks surface to a 4-6 nm layer of
317 hydrophobic alkyl siloxane. Components C1 and C2 impart water resistance, better lubrication
318 for compaction and bonding action bonds at ambient temperature. The existing positive
319 experience refers to silty and clayey soils (Daniels and Hourani, 2009; Ugwu et al., 2013),
320 therefore the research experiments with a new application context. The additive loses its effect
321 in conditions that are seldom achieved in road construction: prolonged exposure to base
322 (Wasserman et al., 1989) or air temperature above 200°C (Kim et al., 2003).

323 The product is mixed at OMC and added to M2 or M3. Two different additive
324 proportions are tested: 1 kg C1 + 1 kg C2 for 200 l water (proportion P1) and 10 kg C1 + 10
325 kg C2 for 200 l water (proportion P2), no special curing procedures are necessary. Proportion
326 P2 has been studied after the initial proportion P1 suggested by the product supplier, since the
327 results regarding P1-treated materials have not been too different from the untreated materials
328 (especially for M3). The materials M2 and M3 enhanced performances are assessed by RTLts.
329 Furthermore, the beneficial coating effect promoted by the additive is evaluated by the standard
330 procedures in terms of resistance against fragmentation (LA test) and wearing (MDE test). In
331 this case, materials M2 and M3 are soaked with the additive (50% C1, 50% C2) and tested after
332 24 hours to let the crushed rocks dry.

333

334 **2.2.3 LIGNIN-BASED ADDITIVE APPLICATION**

335

336 The lignin-based additive (also referred to as lignosulfonate) is a renewable product of pulp
337 and paper industry. It comes from lignin, which is generated by extracting fiber and wood pulp
338 from plant biomass; lignin global annual production is approximately equal to 50 million tons
339 (Angenent et al., 2004). Lignosulfonate is an organic polymer that consists of both hydrophilic
340 and hydrophobic groups; it is a non-corrosive and non-toxic chemical (Alazigha et al., 2018).
341 Previous experiments investigating the strength and density modification of unpaved road
342 using lignosulfonate showed promising outcomes for silty and clayey soils (Alazigha et al.,
343 2018; Chen et al., 2014; Santoni et al., 2002; Ta'negonbadi and Noorzad, 2018; Zhang et al.,
344 2018). As in the case for the polymer-based additive, the product application to crushed rocks
345 could bring to a wider acceptance of this admixture.

346 The product is mixed at OMC and added to M2 or M3; the mass percentage of
347 lignosulfonate added to the crushed rocks is 1.5%. RTLts assess the materials M2 and M3
348 enhanced performances. Lignosulfonate needs a curing time to dry in order to become effective
349 and attach properly to the material particles (Santoni et al., 2002). To simulate a long field

350 curing process, each RTL sample is firstly conditioned at 50°C for 24 hours and then at 22°C
 351 (room temperature) for 24 hours before testing. LA and MDE tests assess the beneficial coating
 352 effect provided by the lignin-based additive. Materials M2 and M3 are soaked with the product
 353 and undergo the same curing procedure.

354

355 2.2.4 OVERHEATING

356

357 The temperature sensitivity of rocks is subject to the geological formation process and
 358 mineralogical composition; they can achieve increased mechanical strength by heating (Zhang
 359 et al., 2009). Research done on diabase shows an enhanced compressive strength after heating
 360 at 190°C and 345°C compared to the investigation results referring to 27°C and 110°C
 361 (Simpson and Fergus, 1968). Another study is related to drying six different rocks (marble,
 362 limestone, granite, slate and two sandstones) with a temperature higher than 100 °C: an
 363 irreversible average 6% increase in the compressive strength properties is attained (Obert et al.,
 364 1946). These experiences prove that exposing the materials to high temperatures may change
 365 the original mechanical strength. Materials M2 and M3 are conditioned at 175°C and 250°C
 366 for 24 hours and 48 hours. After cooling down, micro-Deval standard tests are accomplished.

367

368 3 TEST RESULTS AND DISCUSSION

369

370 3.1 MIXTURE OF THE ROCKS AVAILABLE IN SITU

371

372 Three proportions in mass (25%, 50%, 75%) of “weak” material M2 or M3 are tested in
 373 combination with “strong” material M1. Figure 6a and Figure 6b display the results for M2 and
 374 M3 respectively.

375

376

377

378

379

380

381

382

383

384

385

386

387

388

389

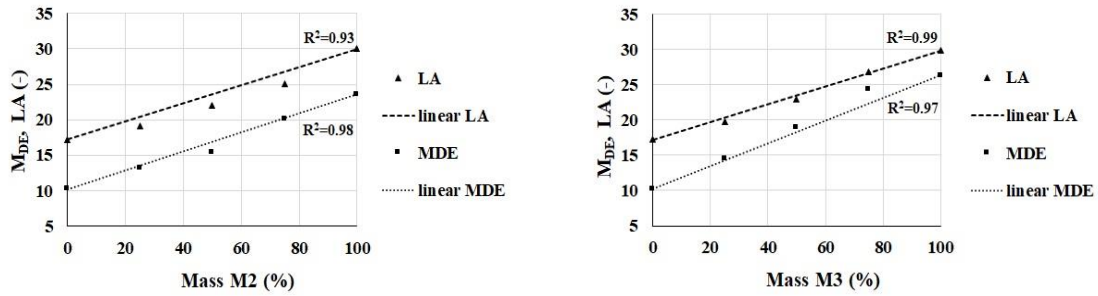
390

391

392

393

394



385 Fig. 6. LA and MDE results and linear trend distributions
 386 for mixtures made of M2 and M1 (a), M3 and M1 (b).

388 The results distribution highlights a linear trend regarding both LA and MDE tests. The
 389 following equations describe the observed data in a mixture made of two materials i and j

390

$$391 LA_{i+j} = LA_i \frac{m_i}{m_i+m_j} + LA_j \frac{m_j}{m_i+m_j}, \quad (5)$$

392

$$393 M_{DE,i+j} = M_{DE,i} \frac{m_i}{m_i+m_j} + M_{DE,j} \frac{m_j}{m_i+m_j}; \quad (6)$$

394

395 where m_i, m_j are the masses and $LA_i, LA_j, M_{DE,i}, M_{DE,j}$ are the standard test values assessed for
 396 materials i, j . A proper mixture of different crushed rocks types is an effective method to meet
 397 the code requirements and, possibly, to maximize the use of the “weak” material.

398 This requires an extra processing step and space to store the two (or more) qualities of
 399 rock; on the other hand, the clear linear results for different combinations should bolster a stable
 400 production: the economic feasibility has to be evaluated depending on the local specific
 401 conditions. The mixed materials are not tested in the RTLTL device, but it is reasonable to
 402 believe that the mechanical properties show similar linear trends.

403

404 3.2 POLYMER-BASED ADDITIVE APPLICATION

405

406 RTLTLs assess the stiffness and the deformation properties of the investigated materials at OMC
 407 $w=5\%$; the behaviour of untreated M1, M2 and M3 serves as a comparison basis. Figure 7a
 408 displays the bulk density and dry density at OMC, Figure 7b illustrates the bulk density after
 409 the addition of the polymer-based product according to proportions P1, P2.

410

411

412

413

414

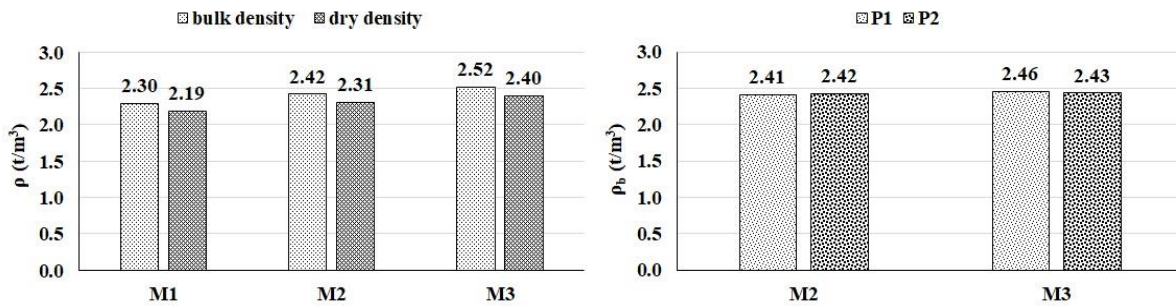
415

416

417

418

419



420 Fig. 7. M1, M2 and M3 bulk density and dry density at OMC $w=5\%$ (a),
 421 M2 and M3 bulk density after additive application with P1, P2 proportions (b).
 422

423 Resilient modulus $k-\theta$ relationships are evaluated (equation 2) through data regression, Figure
 424 8 displays the results. Figure 8a shows the performance of M1, M2 and M3 at OMC without
 425 additive; material M1 is stiffer than materials M2 and M3. Figure 8b illustrates the enhanced
 426 behaviour of M2 and M3: they get stiffer when changing from proportion P1 to proportion P2;
 427 the “weak” rocks performance becomes comparable with the “strong” rocks behaviour. The
 428 results show the product is more effective on M2 than M3 probably because of the geological
 429 composition. The additive performance is dependent on the quantity of silicate minerals on the
 430 rocks surface. M2 and M3 have similar content of quartz and feldspar, but M2 is richer in
 431 amphibole and with a more distinct content of mica. M3 has a higher content of epidote-zoisite,
 432 which has lower Si-contents, as well as calcite ($CaCO_3$) which does not contain silicon.

433

434

435

436

437

438

439

440

441

442
 443
 444
 445
 446
 447
 448
 449
 450
 451
 452
 453
 454
 455
 456
 457
 458
 459
 460
 461
 462
 463
 464
 465
 466
 467
 468
 469
 470
 471
 472
 473
 474
 475
 476
 477
 478
 479
 480
 481
 482
 483
 484
 485
 486
 487

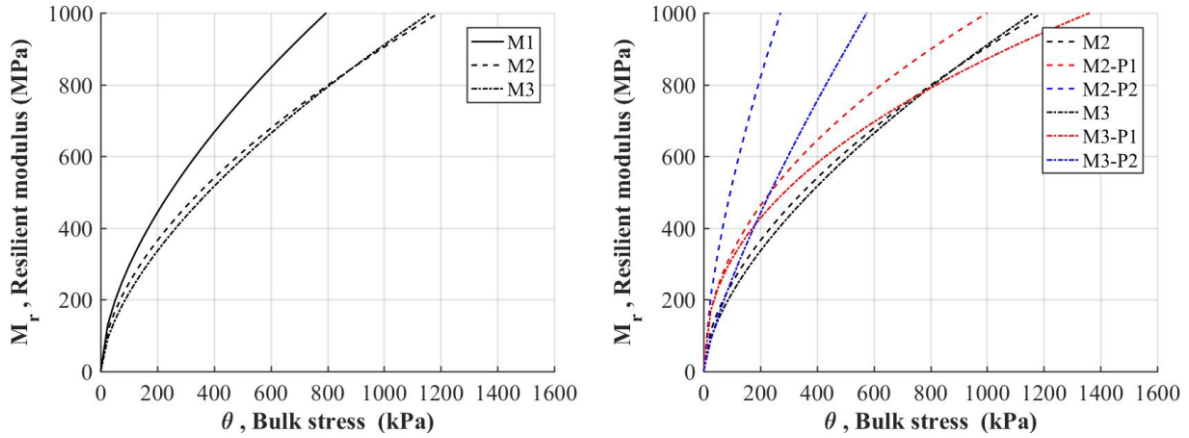


Fig. 8. M1, M2 and M3 resilient modulus at OMC $w=5\%$ (a),
 M2 and M3 resilient modulus after additive application with P1, P2 proportions (b).

The additive effects also pertain to the deformation properties of the materials. Figure 9 depicts the mobilized angle of friction ρ and the angle of friction at incremental failure ϕ for the crushed rocks without and with the polymer-based stabilization; the additive application enhances both the angles.

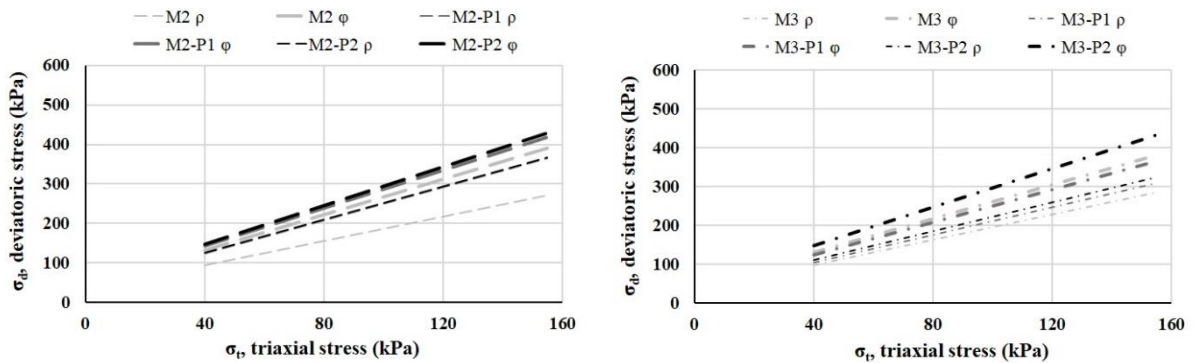


Fig. 9. Mobilized angle of friction ρ and angle of friction at incremental failure ϕ of M2 (a)
 and M3 (b) for untreated and additive-treated conditions.

Table 2 reports the k - θ model regression parameters and the values of the boundary angles.

Material	Model parameters		R^2	Limit angles	
	k_1	k_2		ρ	φ
M1	2994	0.59	0.99	58.4	64.9
M2	2467	0.56	0.99	57.2	65.8
M2-P1	3314	0.48	0.99	64.4	67.3
M2-P2	5206	0.65	0.99	64.6	67.8
M3	2184	0.62	0.99	58.5	65.3
M3-P1	3142	0.44	0.99	60.4	64.4
M3-P2	2576	0.78	0.99	61.6	68.0

Table 2. Regression parameters of M_R model and ρ , φ angles for M1, M2 and M3.

LA and MDE standard tests are used to assess the coating effect provided by the polymer-based product. Figure 10 shows that the additive supplies a significant beneficial effect when it comes to MDE wearing, it also provides a lesser benefit regarding the LA fragmentation. The steel balls used in the LA test imply higher impact loads compared to MDE test; therefore, the thin coating protection is more effective in the latter case.

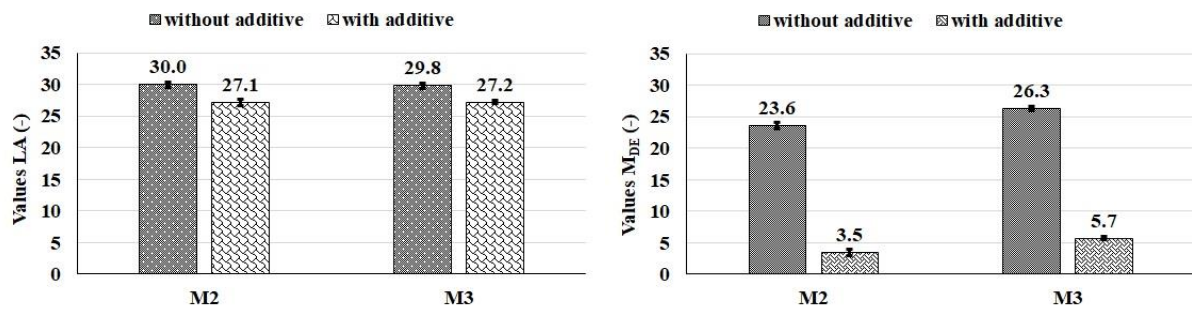


Figure 10. Coating effect provided by the polymer-based additive assessed by standard procedures: LA test (a) and MDE test (b).

3.3 LIGNIN-BASED ADDITIVE APPLICATION

RTLs assess the stiffness and the deformation properties of the investigated materials, which are mixed with 1.5% lignosulfonate in mass at OMC $w=5\%$; the measured water contents after the curing process are between 2% and 2.5%. The behaviour of the untreated materials at $w=1\%$ serves as a comparison basis, this is a cautious comparison since M_R gradually reduces as w increases (Erlingsson et al., 2017). Figure 11a displays the bulk density and dry density at $w=1\%$, Figure 11b illustrates the bulk density relative to the main stages of the curing process after additive application.

526
 527
 528
 529
 530
 531
 532
 533
 534
 535
 536
 537
 538
 539
 540
 541
 542
 543
 544
 545
 546
 547
 548
 549
 550
 551
 552
 553
 554
 555
 556
 557
 558
 559
 560
 561
 562
 563
 564
 565
 566
 567
 568
 569
 570
 571

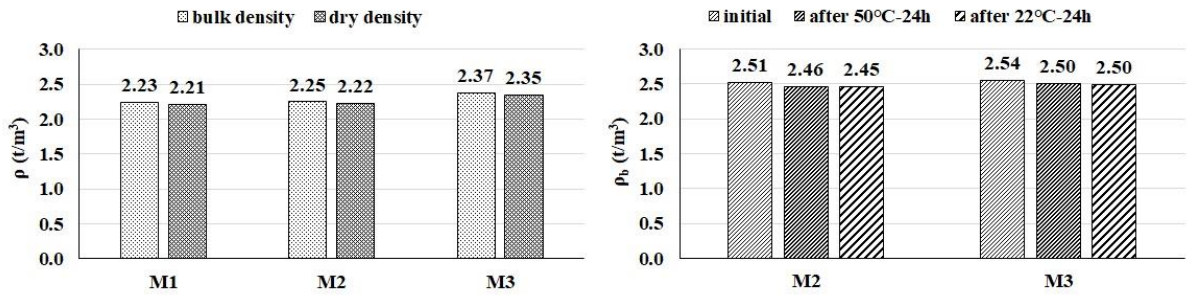


Fig. 11. M1, M2 and M3 bulk density and dry density at w=1% (a),
 M2 and M3 bulk density after additive application (b).

Resilient modulus k- θ relationships are evaluated (equation 2) through data regression, Figure 12 displays the results. Figure 12a shows the performance for M1, M2 and M3 at w=1%; material M1 is stiffer than M2 and M3. Figure 12b illustrates the enhanced stiffer resilient curves of materials M2 and M3.

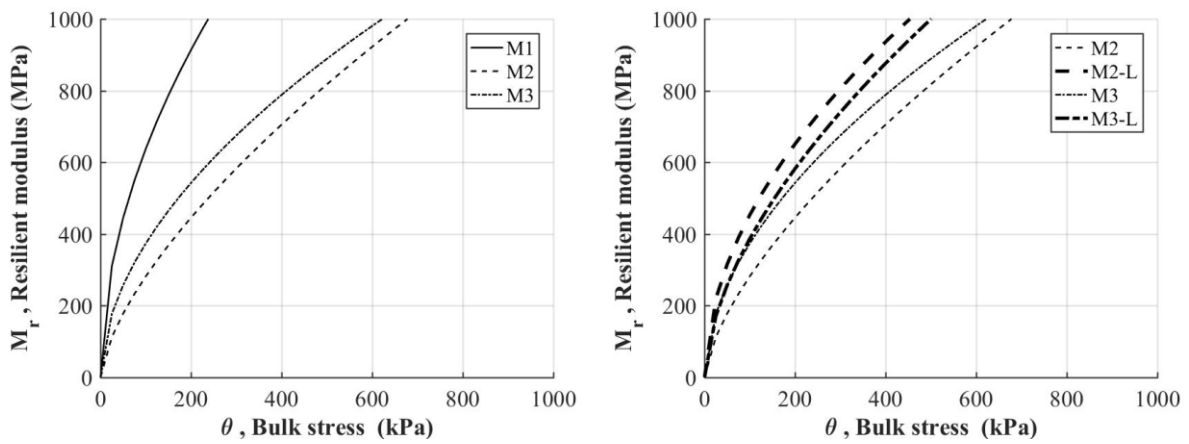


Fig. 12. M1, M2 and M3 resilient modulus at w=1% (a),
 M2 and M3 resilient modulus after additive application (b).

The additive effects also pertain to the deformation properties of the materials. Figure 13 depicts the mobilized angle of friction ρ and the angle of friction at incremental failure ϕ for the crushed rocks without and with the lignin-based stabilization; the additive application enhances both the angles.

572
 573
 574
 575
 576
 577
 578
 579
 580
 581
 582
 583
 584
 585
 586
 587
 588
 589
 590
 591
 592
 593
 594
 595
 596
 597
 598
 599
 600
 601
 602
 603
 604
 605
 606
 607
 608
 609
 610
 611

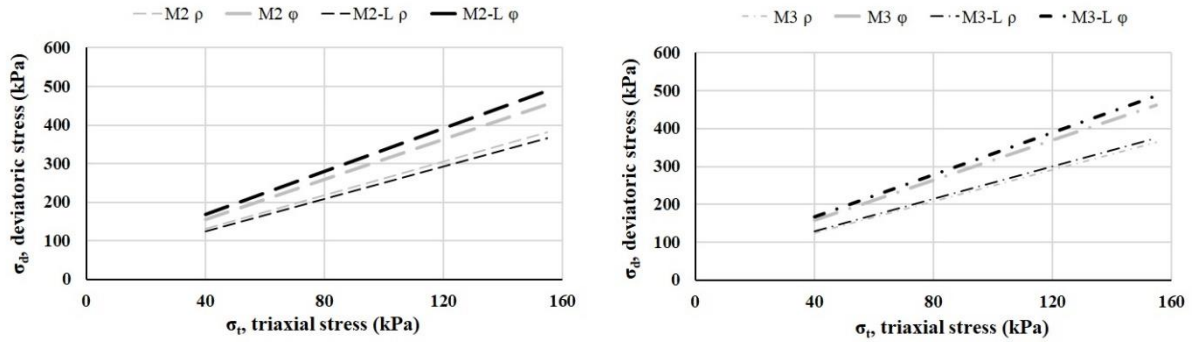


Fig. 13. Mobilized angle of friction ρ and angle of friction at incremental failure ϕ of M2 (a) and M3 (b) for untreated and additive-treated conditions.

Table 3 reports the k - θ model regression parameters and the values of the boundary angles.

Material	Model parameters		R^2	Limit angles	
	k_1	k_2		ρ	ϕ
M1	6378	0.52	0.99	62.1	67.3
M2	2816	0.66	0.99	65.4	68.9
M2-L	4530	0.52	0.99	64.4	70.3
M3	3737	0.54	0.99	64.3	69.2
M3-L	3869	0.59	0.99	65.0	70.2

Table 3. Regression parameters of M_R model and ρ , ϕ angles for M1, M2 and M3.

LA and MDE standard tests are used to assess the coating effect when soaked with the lignin-based additive. Figure 14 shows that the product provides a beneficial effect in terms of LA fragmentation; there is also a small enhancement in terms of MDE wearing. The improvement in MDE values is not as pronounced as one would expect because lignosulfonate is highly moisture susceptible (Santoni et al., 2002); this property is especially relevant when referring to running water, as in the case of MDE test.

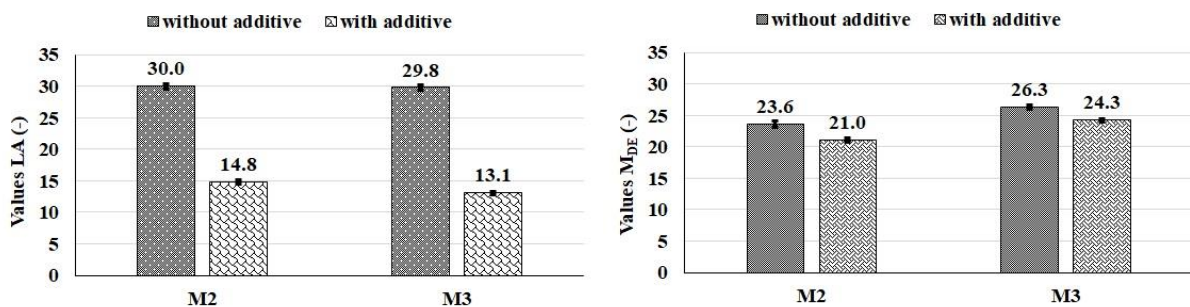


Figure 14. Coating effect provided by the lignin-based additive assessed by standard procedures: LA test (a) and MDE test (b).

612 3.4 OVERHEATING

613

614 Materials M2 and M3 are tested with the MDE procedure to assess if the overheating can induce
615 modifications in the mineralogical structure, which may strengthen the rocks and improve the
616 MDE results. The values of the three tested conditioning temperatures (105°C, 175°C, 250°C)
617 do not seem to exert a major influence. On the other hand, the duration of the overheating
618 seems to be a more relevant factor, as the results connected to the 48-hour conditioning are
619 better than those connected to the 24-hour conditioning (Figure 15). Even so, the induced
620 improvement is considerably limited as the highest observed decrease among the original MDE
621 values is equal to approximately two units. The tested conditioning temperatures do not
622 significantly improve the weak materials to make them meet the code requirements. Anyway,
623 overheating the crushed rocks would demand an intensive energy use even if a small beneficial
624 effect was found.

625

626

627

628

629

630

631

632

633

634

635

636

637

638

639

640

641

642

643

644

645

646

647

648

649

650

651

652

653

654

655

656

657

658

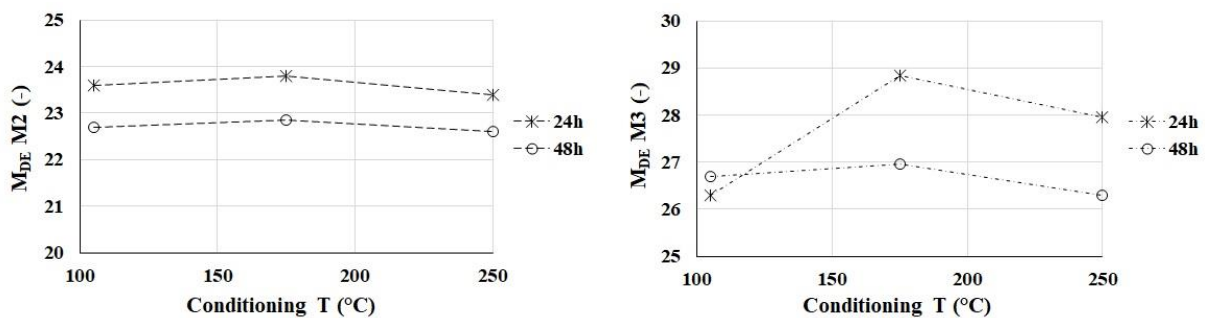


Fig. 15. MDE values after overheating M2 (b) and M3 (b).

636 4 CONCLUSIONS

637

638

639

640

641

642

643

644

645

646

647

648

649

650

651

652

653

654

655

656

657

658

The research investigated different approaches to improve the mechanical properties of crushed rocks to serve as construction materials in the road unbound layers. Three types of crushed rocks M1, M2 and M3 were tested; M1 satisfies the code requirements, while M2 and M3 do not meet them. The following conclusions can be drawn; they could be generalized by further testing of more materials:

- (1) Both RTLTs and LA, MDE tests identify that material M1 has a better performance than materials M2 and M3. RTLTs can also assess the beneficial effect of the additive; on the other hand, there are no standard LA and MDE test procedures concerning an additive application.
- (2) An appropriate mixture of the crushed rocks available in situ may represent a convenient solution to fulfil LA and MDE requirements. The LA and MDE values of the mixture can be evaluated by a linear relationship based on the mass quantity of each employed material.
- (3) The pavement design code does not prohibit mixing different materials and certifying the obtained admixture as the chosen construction material. However, it is possible that weaker grains might be exposed to extra wear and/or crushing when they are mixed with the strong particles, especially if the difference in LA/MDE is large. In addition, there may be practical problems when it comes to securing a good mix and avoid segregation.

659 (4) Both polymer-based additive and lignin-based additive are non-traditional stabilization
660 approaches to improve the mechanical properties of crushed rocks and enable their use in the
661 pavement unbound layers. The investigated additives coat and bond the material particles
662 closely together; the polymer-based product has a rapid effect, the lignin-based product needs
663 a curing time.

664

665 (5) The effect of the polymer-based additive is dependent on the silicate content of the rocks
666 surface. The lignin-based additive application may need to consider the environmental
667 conditions, as it is water susceptible. A suitable solution could be to apply this admixture during
668 days without rainfall and then cover the treated layer with a top (e.g. bituminous) layer; another
669 option could be to make sure that the water can properly drain (e.g. good profile and well-
670 maintained ditches).

671

672 (6) The promising results obtained by laboratory tests and discussed in this study should be
673 further investigated, for instance by means of a field-test campaign. Furthermore, repeating the
674 measurements after a long time interval may be useful to assess the long-term response of the
675 stabilizing products and assessing the possible formation of micro plastics on the surface.

676

677 (7) The attained overheating procedure does not produce a substantial improvement in the
678 materials performance.

679

680 **ACKNOWLEDGMENTS**

681

682 This work has been supported by Norwegian Public Roads Administration (grant number
683 25134404). Polymer-based additive kindly supplied by Sparks AS, Asker, Norway and Zydex
684 Industries, Vadodara, India. Lignin-based additive kindly supplied by Borregaard AS,
685 Sarpsborg, Norway.

686 **REFERENCES**

687
688
689
690
691
692
693
694
695
696
697
698
699
700
701
702
703
704
705
706
707
708
709
710
711
712
713
714
715
716
717
718
719
720
721
722
723
724
725
726
727
728
729
730
731
732
733
734
735

1. Aatheesan T, Arulrajah A, Wilson J, Bo MW. Beneficial use of brick rubble as pavement sub-base material. *Adv. Transp. Geotech.*, London: Taylor & Francis; 2008, p. 695–9.
2. Alazigha DP, Indraratna B, Vinod JS. Mechanisms of stabilization of expansive soil with lignosulfonate admixture. *Transp Geotech* 2018;14:81–92. doi:10.1016/J.TRGEO.2017.11.001.
3. Angenent LT, Karim K, Al-Dahhan MH, Wrenn BA, Domínguez-Espinosa R. Production of bioenergy and biochemicals from industrial and agricultural wastewater. *Trends Biotechnol* 2004;22:477–85. doi:10.1016/j.tibtech.2004.07.001.
4. Arulrajah A, Mohammadinia A, Horpibulsuk S, Samingthong W. Influence of class F fly ash and curing temperature on strength development of fly ash-recycled concrete aggregate blends. *Constr Build Mater* 2016;127:743–50. doi:10.1016/j.conbuildmat.2016.10.049.
5. Arulrajah A, Piratheepan J, Disfani MM, Bo MW. Geotechnical and geoenvironmental properties of recycled construction and demolition materials in pavement subbase applications. *J Mater Civ Eng* 2013;25:1077–88. doi:10.1061/(ASCE)MT.1943-5533.0000652.
6. Barbieri DM, Hoff I, Mork H. Laboratory investigation on unbound materials used in a highway with premature damage. 10th Int. Conf. Bear. Capacit. Roads, Railw. Airfields, 2017.
7. Barbieri DM, Hoff I, Mørk MBE. Mechanical assessment of crushed rocks derived from tunnelling operations. In: Cheng W-C, Yang J, Wang J, editors., Springer; 2019, p. 225–41. doi:https://doi.org/10.1007/978-3-319-95783-8_19.
8. Barksdale RD. Compressive stress pulse times in flexible pavements for use in dynamic testing. *Highw. Res. Rec.*, 1971, p. 32–44.
9. Behnood A. Soil and clay stabilization with calcium- and non-calcium-based additives: a state-of-the-art review of challenges, approaches and techniques. *Transp Geotech* 2018;17:14–32. doi:10.1016/j.trgeo.2018.08.002.
10. Berger A. Massedeponering. Beregning av kostnadsminimale transportmønstre for planering av fjell- og jordmasser ved bygging av veier. Norwegian University of Science and Technology, 1978.
11. Burdin J, Monin N. The management of excavated materials from the Lyon-Turin rail link project. *Geomech Und Tunnelbau* 2009;2:652–62. doi:10.1002/geot.200900048.
12. CEN. Tests for geometrical properties of aggregates. Part 1: determination of particle size distribution. Sieving method. 2012a.
13. CEN. Tests for mechanical and physical properties of aggregates. Part 3: determination of particle shape - flakiness index. 2012b.
14. CEN. Tests for mechanical and physical properties of aggregates. Part 1: determination of the resistance to wear (micro-Deval). 2011.
15. CEN. Tests for mechanical and physical properties of aggregates. Part 2: methods for the determination of resistance to fragmentation. 2010.
16. CEN. Cyclic load triaxial test for unbound mixture. 2004.
17. CEN. Unbound and hydraulically bound mixtures. Part 4: test methods for laboratory reference density and water content. Vibrating hammer. 2003.
18. Chen Q, Indraratna B, Carter J, Rujikiatkamjorn C. A theoretical and experimental study on the behaviour of lignosulfonate-treated sandy silt. *Comput Geotech* 2014;61:316–27. doi:10.1016/j.compgeo.2014.06.010.
19. Chittoori B, Puppala AJ, Reddy R, Marshall D. Sustainable reutilization of excavated

- trench material. *GeoCongress 2012* 2012:4280–9. doi:10.1061/9780784412121.440.
- 737 20. Daniels J, Hourani MS. Soil improvement with organo-silane. U.S.-China Work. Gr.
738 Improv. Technol. 2009, Orlando: 2009. doi:doi.org/10.1061/41025(338)23.
- 739 21. Dongmo-Engeland B. GARAP, Influence of sample's height on the development of
740 permanent deformation. Trondheim: 2005.
- 741 22. Dunham KK. Coastal Highway Route E39 - Extreme crossings. *Transp Res Procedia*
742 2016;14:494–8. doi:10.1016/j.trpro.2016.05.102.
- 743 23. Erichsen E, Ulvik A, Sævik K. Mechanical degradation of aggregate by the Los
744 Angeles-, the micro-Deval- and the nordic test methods. *Rock Mech Rock Eng*
745 2011;44:333–7. doi:10.1007/s00603-011-0140-y.
- 746 24. Erlingsson S, Rahman MS, Salour F. Characteristic of unbound granular materials and
747 subgrades based on multi stage RLT testing. *Transp Geotech* 2017;13:28–42.
748 doi:10.1016/j.trgeo.2017.08.009.
- 749 25. Fladvad M, Aurstad J, Wigum BJ. Comparison of practice for aggregate use in road
750 construction - results from an international survey. 10th Int. Conf. Bear. Capacit.
751 Roads, Railw. Airfields, 2017.
- 752 26. Gomes Correia A, Winter MG, Puppala AJ. A review of sustainable approaches in
753 transport infrastructure geotechnics. *Transp Geotech* 2016;7:21–8.
754 doi:10.1016/j.trgeo.2016.03.003.
- 755 27. Haritonovs V, Tihonovs J, Smirnovs J. High modulus asphalt concrete with dolomite
756 aggregates. *Transp Res Procedia* 2016;14:3485–92. doi:10.1016/j.trpro.2016.05.314.
- 757 28. Hicks RG, Monismith CL. Factors influencing the resilient properties of granular
758 materials. *Highw. Res. Rec.*, 1971, p. 15–31.
- 759 29. Hoff I, Bakløkk LJ, Aurstad J. Influence of laboratory compaction method on
760 unbound granular materials. 6th Int. Symp. Pavements Unbound, 2003.
- 761 30. Huang Y, Wang L. Experimental studies on nanomaterials for soil improvement: a
762 review. *Environ Earth Sci* 2016;75:497. doi:10.1007/s12665-015-5118-8.
- 763 31. Jiang YJ, Fan LF. An investigation of mechanical behavior of cement-stabilized
764 crushed rock material using different compaction methods. *Constr Build Mater*
765 2013;48:208–515. doi:10.1016/j.conbuildmat.2013.07.017.
- 766 32. Kim HK, Lee JP, Park CR, Kwak HT, Sung MM. Thermal decomposition of
767 alkylsiloxane self-assembled monolayers in air. *J Phys Chem B* 2003;107:4348–51.
768 doi:10.1021/jp022377s.
- 769 33. Lekarp F, Isacsson U, Dawson A. State of the art. I: resilient response of unbound
770 aggregates. *J Transp Eng* 2000a;126:66–75. doi:https://doi.org/10.1061/(ASCE)0733-
771 947X(2000)126:1(66).
- 772 34. Lekarp F, Isacsson U, Dawson A. State of the art. II: permanent strain response of
773 unbound aggregates. *J Transp Eng* 2000b;126:76–83. doi:10.1061/(ASCE)0733-
774 947X(2000)126:1(76).
- 775 35. Lieb R. Materials management at the Gotthard base tunnel - experience from 15 years
776 of construction. *Geomech Und Tunnelbau* 2009;2:619–26.
777 doi:10.1002/geot.200900032.
- 778 36. Mohammadinia A, Arulrajah A, Haghghi H, Horpibulsuk S. Effect of lime
779 stabilization on the mechanical and micro-scale properties of recycled demolition
780 materials. *Sustain Cities Soc* 2017;30:58–65. doi:10.1016/j.scs.2017.01.004.
- 781 37. Myre J. The use of cold bitumen stabilized base course mixes in Norway 2014:1–14.
- 782 38. Neeb P-R. Byggeråstoff. Trondheim: Tapir; 1992.
- 783 39. NGU. Norges Geologiske Undersøkelse (Geological Survey of Norway) 2017.
784 <http://www.ngu.no/> (accessed September 10, 2018).
- 785 40. NPRA. The E39 coastal highway route 2017.

- 786 <https://www.vegvesen.no/en/roads/Roads+and+bridges/Road+projects/e39coastalhigh>
787 [wayroute;jsessionid=99D143CB28F87A072777C744BBCA31E8?lang=nn](https://www.vegvesen.no/en/roads/Roads+and+bridges/Road+projects/e39coastalhigh) (accessed
788 September 10, 2018).
- 789 41. NPRA. Håndbok N200 vegbygging. Norway: Vegdirektoratet; 2014a.
 - 790 42. NPRA. Kalde bitumen- stabiliserte bærelag. Norway: Vegdirektoratet; 2014b.
 - 791 43. Núñez WP, Ceratti JA, Malysz R, Retore TS. Using unbound aggregates resulting
792 from amethyst mining in low volume roads. *Adv. Transp. Geotech.*, London: Taylor
793 & Francis; 2008, p. 219–25.
 - 794 44. Obert L, Windes SL, Duvall WI. Standardized tests for determining the physical
795 properties of mine rock. 1946.
 - 796 45. Paul DR, Robeson LM. Polymer nanotechnology: nanocomposites. *Polymer (Guildf)*
797 2008;49:3187–204. doi:10.1016/j.polymer.2008.04.017.
 - 798 46. Petkovic G. Recycling in Norwegian conditions. In: Nordal RS, Refsdal G, editors.
799 5th Int. Conf. Bear. Capacit. Roads Airfields, Trondheim: Tapir; 2005.
 - 800 47. Ramberg IB, Bryhni I, Nøttvedt A, Rangnes K. Landet blir til. Trondheim: 2013.
 - 801 48. Resch D, Lassnig K, Galler R, Ebner F. Tunnel excavation material - high value raw
802 material. *Geomech Und Tunnelbau* 2009;2:612–8. doi:10.1002/geot.200900047.
 - 803 49. Riviera PP, Bellopede R, Marini P, Bassani M. Performance-based re-use of tunnel
804 muck as granular material for subgrade and sub-base formation in road construction.
805 *Tunn Undergr Sp Technol* 2014;40:160–73. doi:10.1016/j.tust.2013.10.002.
 - 806 50. Roco MC. Broader societal issues of nanotechnology. *J Nanoparticle Res*
807 2003;5:181–9. doi:10.1023/A:1025548512438.
 - 808 51. Santoni RL, Tingle JS, Webster SL. Stabilization of silty sand with nontraditional
809 additives. *Transp Res Rec* 2002:61–70.
 - 810 52. Simpson DR, Fergus JH. The effect of water on the compressive strength of diabase
811 1968;73:6591–4.
 - 812 53. Siripun K, Jitsangiam P, Nikraz H. Characterization analysis and design of hydrated
813 cement treated crushed rock base as a road base material in Western Australia. *Int J*
814 *Pavement Res Technol* 2010;10:39–47. doi:10.1080/10298430802342682.
 - 815 54. Sobolev K, Shah SP. Nanotechnology in construction. In: Sobolev K, Shah SP,
816 editors. *Proc. NICOM5*, Springer; 2015, p. 509. doi:10.1007/978-3-319-17088-6.
 - 817 55. Ta'negonbadi B, Noorzad R. Physical and geotechnical long-term properties of
818 lignosulfonate-stabilized clay: An experimental investigation. *Transp Geotech*
819 2018;17:41–50. doi:10.1016/j.trgeo.2018.09.001.
 - 820 56. Teknologirådet. Teknologirådet | Norge 2030 arkiver 2012.
821 <https://teknologiradet.no/norge-2030/> (accessed September 10, 2018).
 - 822 57. Ugwu OO, Arop JB, Nwoji CU, Osadebe NN. Nanotechnology as a preventive
823 engineering solution to highway infrastructure failures. *J Constr Eng Manag*
824 2013;139:987–93. doi:10.1061/(ASCE)CO.1943-7862.0000670.
 - 825 58. Uthus L, Tutumluer E, Horvli I, Hoff I. Influence of grain shape and texture on the
826 deformation properties of unbound aggregates in pavements. *Int J Pavements* 2007;6.
 - 827 59. Wasserman SR, Tao YT, Whitesides GM. Structure and reactivity of alkylsiloxane
828 monolayers formed by reaction of alkyltrichlorosilanes on silicon substrates.
829 *Langmuir* 1989;5:1074–87. doi:10.1021/la00088a035.
 - 830 60. Zhang L, Mao X, Lu A. Experimental study on the mechanical properties of rocks at
831 high temperature. *Sci China, Ser E Technol Sci* 2009;52:641–6. doi:10.1007/s11431-
832 009-0063-y.
 - 833 61. Zhang T, Cai G, Liu S. Application of lignin-stabilized silty soil in highway subgrade:
834 A macroscale laboratory study. *J Mater Civ Eng* 2018;30.
835 doi:10.1061/(ASCE)MT.1943-5533.0002203.

836 **AUTHORS' BIOGRAPHIES**

837
838
839
840
841
842
843
844
845
846
847



848 **Diego Maria Barbieri** is currently Ph.D. Candidate at Norwegian University of Science and
849 Technology, Norway. Before joining the Ph.D. program, he obtained the 2nd level postgraduate
850 master and specialization diploma in railway engineering at La Sapienza University, Italy. He
851 obtained his bachelor and master degree in Civil Engineering at University of Modena and
852 Reggio Emilia, Italy; during this period, he had the opportunity to deepen his studies at Fuzhou
853 University, PRC, as a visiting scholar. His research areas mainly comprise pavement
854 engineering; he is particularly interested in investigating sustainable solutions for infrastructure
855 construction.

856
857
858
859
860
861
862
863
864
865



866 Professor Dr. **Inge Hoff** has been doing research on materials for road, railway constructions
867 and pavement design, especially use of unbound granular materials, for more than 20 years.
868 His research interest is both on experimental work in laboratory or field and numerical
869 modelling and design of roads and railways. Before starting to work as professor at NTNU nine
870 years ago, he had been working at the independent research organization SINTEF.

871
872
873
874
875
876
877
878
879
880
881



882 Professor Dr. **Mai Britt E. Mørk** started as professor in geology at NTNU Department of
883 Geology and Mineral Resources Engineering in 2003, now Department of Geoscience and
884 Petroleum. She has geological background from University of Oslo and several years at
885 SINTEF.